



Research paper

Characteristics of sandstone unloading creep and modelling for safe tunnel construction under high perimeter pressure and high pore water pressure condition

Li Song¹, Fujun Tang², Dehui Kong³

Abstract: Research on the properties of sandstone in the tunnel environment has been conducted due to the building industry's rapid development, which is gradually involving underground water. Sandstone used in tunnel construction is susceptible to high perimeter and water pressures as a result of the abundance of sand and gravel close to groundwater, which might result in mishaps resembling collapses. The modified Burgers Model for the Malm dataset is the foundation of this study, which aims to reduce the internal crack extension caused by sandstone's unloading creep. First, the study increased the material's Poisson's ratio in accordance with the Mohr–Coulomb strength criterion and builds a triaxial loading model on its foundation. Next, it analyzed the extension of the fracture surface of sandstone while taking high peripheral pressure and high hydraulic pressure into account. Finally, it discretized the unloading creep of sandstone using the improved Burgers model. On the basis of the model put forward in the study, experimental validation was then done on the Malm dataset. The sandstone would reach the final rupture area without any protection measures in just 10 days, but the model suggested in the study can delay this time to 200 days, while the effects of the other three models would delay this time by 75, 60, and 41 days, respectively. The model's breadth was indicated by the linear fit value of 0.9827 for 36 experiments. The experimental findings demonstrated that the model suggested in the study can successfully lower the rate of sandstone unloading creep and increase worker safety.

Keywords: burgers model, confining pressure, MC strength criterion, pore water pressure, rupture surface, unloading creep

¹MsC., Department of Road and Bridge Engineering, Sichuan Vocation and Technical College of Communications, Chengdu, 611130, China, e-mail: sli202202@163.com, ORCID: [0009-0002-6704-2240](https://orcid.org/0009-0002-6704-2240)

²MsC., Department of Road and Bridge Engineering, Sichuan Vocation and Technical College of Communications, Chengdu, 611130, China, e-mail: sct2000320048@163.com, ORCID: [0009-0003-1469-1498](https://orcid.org/0009-0003-1469-1498)

³MsC., School of Civil Engineering, Southwest Jiaotong University, Chengdu, 610031, China, e-mail: kdehui596@126.com, ORCID: [0000-0002-0970-195X](https://orcid.org/0000-0002-0970-195X)

1. Introduction

The research focused on staff safety cannot be disregarded against the backdrop of the tunnel construction industry's rapid development, and the researchers' focus is gradually shifting to stress analysis of tunnel sandstone [1, 2]. The sandstone in the tunnel is subjected to high pore water (PW) and high confining pressure (CP) as a result of the construction environment's proximity to the water source and its surrounding abundance of rocks, which results in unloading creep (UC) that cannot be disregarded. UC can alter the strength characteristics of the rock mass, which in turn affects its deformation characteristics, making a previously stable rock mass fragile. This reduction in deformation ability can lead to changes in the pore structure and permeability of the rock mass, making it susceptible to unstable phenomena such as fractures, spalling, or collapse during construction. A complicated geological environment, where rocks deep in the earth's crust have extra physico-chemical characteristics since they are not exposed to air, is present when building underground. The sandstone in this area will experience regular ductility and spreading variations, exhibiting strong extension capacity at high hydraulic pressure and great expansion capacity at high CP, both of which are extremely likely to result in sandstone crushing [3]. The sandstone stress analysis method based on the Burgers Model (BM) has caught the interest of many specialists as a means of lowering sandstone UC in tunnels. The BM is well suited to the working conditions of tunnel construction because to its great adhesive ability and strength requirement. The elastic modulus of plastic sandstone, which introduces a non-negligible inaccuracy in the experimental results, is not taken into account by the model. To address the problem, this study introduces the Mohr–Coulomb (MC) strength criterion to the BM model, resulting in an Improved Burgers Model (IBM). The IBM model analyzes the stress of the tunnel structure and simulates the stability of sandstone during tunnel construction to evaluate the stability of tunnel engineering. The study is divided into four major sections. The first section analyzes and summarizes the current peak strain characteristics and applications of sandstone rupture surface (RS). The second section discusses the risks associated with sandstone UC and introduces the method for building the IBM model. The third section evaluates and contrasts the performance of this optimized model with that of the conventional model. The fourth and final section performs simulation experiments on sandstone. The research has practical applications in mitigating risks associated with tunnel construction. It aims to significantly reduce the UC speed of sandstone under high CP and high water pressure conditions. This can be achieved by following the proposed methodology. This will preserve the geological stability as well as the safety of the construction personnel.

2. Related works

The UC study of sandstone under high CP and hydraulic pressure conditions is getting hot in the context of rapid development of tunneling [4]. Dong et al. observed that the ground in a certain place was raised by 500 mm, and the building above the tunnel was seriously damaged. The experimental results showed that the problem of large confined water in the tunnel requires high viscosity grouting materials to block water for grouting cracks [5]. Jiang et al. conducted

a numerical simulation to analyze the support system of the double-side heading method. The load on its supporting structure was found to be significantly increased. These research findings can provide valuable references for the design of large-section tunnels [6].

Although the UC rate of sandstone is fast in the environment of high CP and PW, the related modeling study also reduces the fracturing rate of sandstone [7]. Wang et al. analyzed the depth of the groundwater table in vegetation, which can help protect groundwater and reduce adverse geological effects in the tunnel construction industry [8]. Zhang analyzed ground settlement in shield construction and established the relationship between ground deformation and construction parameters. The author established the relationship between surface deformation and shield parameters during construction and provided guidance for shield construction [9]. Considering the safety risk of gas tunnel, Qiu and others put forward a risk assessment method of tunnel construction based on Bayesian network. They selected a construction section similar to a tunnel for a case study to verify the application prospect of their method. They established a gas tunnel risk assessment model to let managers avoid the gas tunnel risk [10].

As evidenced by numerous expert studies, models for mitigating sandstone UC are very popular, but little research has been done to optimize the BM. This study pioneered the linking of a triaxial loading model to the BM, which was reconstructed by Poisson's ratio to generate an IBM.

3. Construction of triaxial loading model under the action of high CP and high PW

The triaxial conditions of sandstone under different CP conditions are introduced first, and then the acting force and deformation amplitude are analyzed.

3.1. Experimental modeling of peak strain characterization of RS in sandstone samples

ε^f represents the peak strain, which are calculated as in Eq. (3.1) [11].

$$(3.1) \quad \begin{cases} \varepsilon^f = (l^f - l^0)/l^0 \\ E = (\sigma_1 - 2\mu\sigma_3)/\varepsilon_1 \end{cases}$$

in Eq. (3.1): l^0 , l^f – size of before and after sandstone samples. E – samples related to CP, σ_1 , σ_3 – the axial pressure and CP. μ – Poisson's ratio of the rock sample, ε_1 – its axial strain.

The study uses change of calculating the Poisson's as shown Eq. (3.2) below [12].

$$(3.2) \quad \mu = (B\sigma_1 - \sigma_3)/[\sigma_3(2B - 1) - \sigma_1]$$

in Eq. (3.2): B – ratio of transverse strain to axial strain of rock samples.

It can be seen that PW, CP strain have relationship, as in Eq. (3.3) [13, 14].

$$(3.3) \quad \partial_c = a\sigma_3 \ln(p + 1) + b \ln(p + 1) + c\sigma_3 + d$$

in Eq. (3.3): ∂_c and p – the axial peak strain of the rock sample, a, b, c and d – four sandstone parameters that can be obtained by experiments.

It can be put into the pressure chamber as shown in Fig. 1.

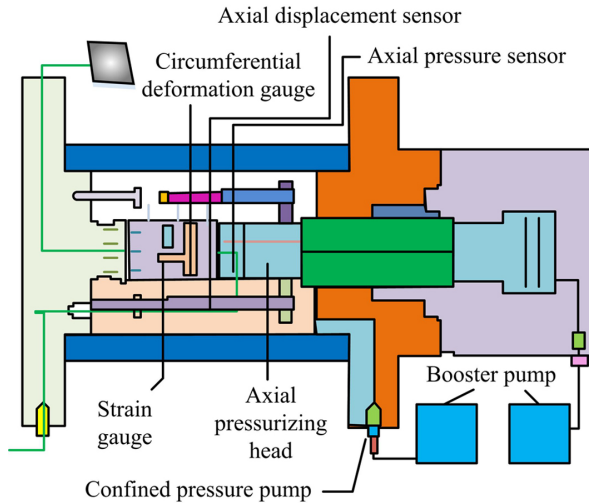


Fig. 1. Diagram of pressure chamber

In the pressure chamber shown in Fig. 1, the principal stress can be expressed by Eq. (3.4). Equation (3.4) constructs the link between the stress and axial pressure and CP of sandstone.

$$(3.4) \quad F(\sigma_1, \sigma_2, \sigma_3) = 0$$

in Eq. (3.4): σ_2 – the principal stress.

This study constructs a triaxial microcell RS of sandstone, as shown in Fig. 2.

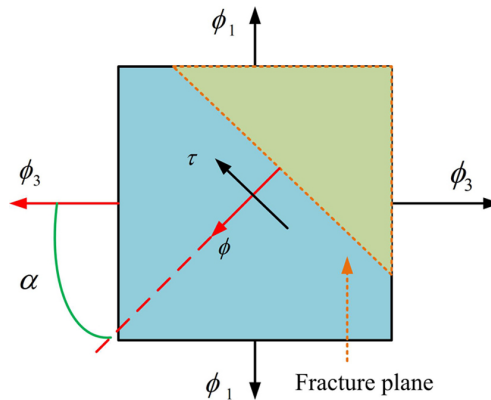


Fig. 2. Stress analysis diagram of fracture surface of triaxial microcell

In Fig. 2, ϕ_3 – the horizontal stress, ϕ_1 – the vertical stress. ϕ, τ – the normal and tangential stresses, α – the acute angle. The relationship between ϕ, τ as in Eq. (3.5) [15].

$$(3.5) \quad \tau = c + \phi \tan \varphi$$

in Eq. (3.5): c – the cohesive force of sandstone and φ – the friction angle within it.

According to the MC damage criterion, and then through Eq. (3.5) the line graph between c and φ can be plotted as shown in Fig. 3.

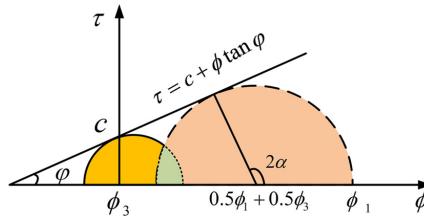


Fig. 3. Relationship diagram between cohesion and friction angle

The critical failure force of sandstone is affected in the experiment, at this time, the static force on the sandstone sample reaches equilibrium, and the connection between positive and normal pressure can be established by Eq. (3.6) [16].

$$(3.6) \quad \begin{cases} \phi = 0.5(\phi_1 + \phi_3) + 0.5(\phi_1 - \phi_3) \cos 2\alpha \\ \tau = 0.5(\phi_1 - \phi_3) \sin 2\alpha \end{cases}$$

in Eq. (3.6): 2α – the sandstone RS inclination.

When the interior of sandstone is covered with damaged pores, its shape changes and the stress intensity decreases accordingly. It is studied to set two parameters to establish a new solution method for sandstone cohesion and friction angle, as shown in Eq. (3.7) [17].

$$(3.7) \quad \begin{cases} \phi = \arcsin \frac{k-1}{k+1} \\ c = \frac{l}{2\sqrt{k}} \end{cases}$$

in Eq. (3.7): $k = (1 + \sin \varphi)/(1 - \sin \varphi), l = 2c \cdot [(1 + \sin \varphi)/(1 - \sin \varphi)]^{0.5}$ – a new method for solving two variables.

As PW rises, there is a negative correlation between both. When sandstone samples are subjected to external stress, a fracture surface will appear once the stress reaches a certain level. The purpose of studying the peak strain characteristics of the fracture surface is to determine the stress and strain levels of the fracture surface. Understanding the UC characteristics can help to comprehend the stress release and deformation behavior of sandstone samples after loading. In practical engineering, rock samples may undergo the cyclic process of loading and unloading. Therefore, it is crucial to understand the creep characteristics of sandstone samples during unloading to predict the stability and reliability of rocks. The study and simulation of the actual stress environment in underground rock, which is often accompanied by high CP and high PW pressure, allows for a more accurate analysis of the formation and development of fracture surfaces.

3.2. Characterization of UC in tunnel sandstone under high CP and high PW conditions

In the mechanical characterization of sandstone, of which the inelastic elements include viscous and semi-viscous ones. The relationship between the applied stress and the spring deformation can be expressed using Eq. (3.8) [18].

$$(3.8) \quad \varpi = E\theta$$

in Eq. (3.8): E – the elasticity coefficient of the spring.

Which is related to the material of the spring. One of the typical viscous slider in line with hydrodynamics, is a common device with viscous piston damping effect, the device stress analysis shown in Fig. 4.

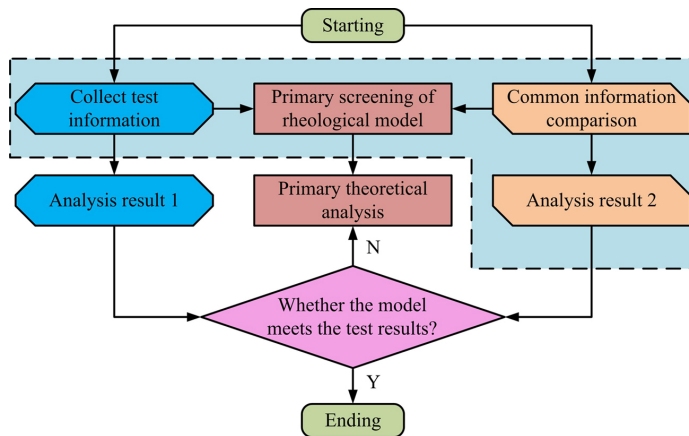


Fig. 4. Diagram of stress analysis of viscous devices

In Fig. 4, the mechanical properties of the spring model. Fig. 4 demonstrates the force analysis of the spring at different temperatures and pressures, Based on this spring extend it to three dimensions as shown in Eq. (3.9) [19].

$$(3.9) \quad \begin{cases} \vartheta_m = 3K\theta \\ S_m = 2Ge \end{cases}$$

in Eq. (3.9): K – the change in volume of the spring, and G – the tension in shearing the spring.

The 3D spring model is taken to be built in a non-linear way, in this study, based on these four modes, a direct screening module and an exclusion module are built, and their microscopic analyses are carried out by the method shown in Fig. 5 [20].

The starting point for Fig. 5 is the rheological characterization of sandstone, as the internal configuration becomes progressively looser over time. This study proposes the use of a damage variable to describe this action, establishing Eq. (3.10) [21].

$$(3.10) \quad \begin{cases} d_E + E/E_0 = 1 \\ d_\eta + \eta/\eta_0 = 1 \end{cases}$$

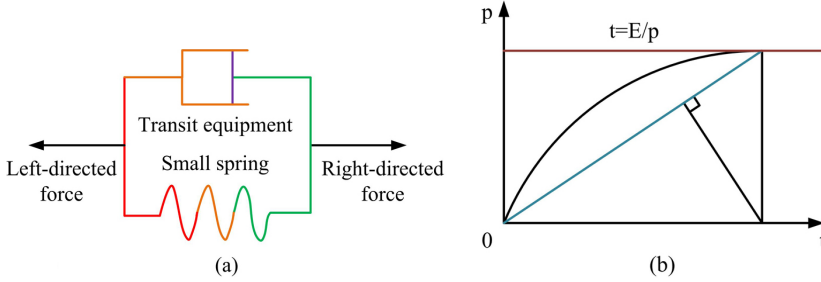


Fig. 5. Flow chart of unloading creep constitutive model of sandstone; (a) Creep stress model of sandstone unloading, (b) Analysis of stress situation

in Eq. (3.10): d_E, d_η – the damage variable and damage efficiency. E_0, η_0 – the modulus of elasticity and viscosity of the initial sandstone, E, η – adjusted values of two parameters of sandstone after water injection is completed.

The sandstone at high CP presents extensional damage. To describe the sandstone’s changing trend with increasing CP water pressure, this study establishes a functional relationship between the two variables, as shown in Eq. (3.11) [22].

$$(3.11) \quad \begin{cases} \sigma_1 = (2c \cos \phi)/(1 - \sin \phi) + (2c\sigma_3 \sin \phi)/(1 - \sin \phi) \\ \sigma_3 = [\sigma_3^B \sin \phi(1 - \sin \phi)^{B-2}]/[2^{B-2}B(nc \cos \phi)^{B-1}] \end{cases}$$

in Eq. (3.11): n – the critical state of sandstone, B – the slope of the function between sandstone and PW.

Since the usual state is $\sigma_1 \leq \sigma_3$, the sandstone stress coincides with the flow law in the plastic state. This study takes into account the PW and the BM, to form the IBM, whose equation of state is shown in Eq. (3.12) [23].

$$(3.12) \quad \begin{cases} \xi_M = E\psi_{M1} \\ \xi_M = \eta\psi_{M2} \\ \xi_K = K\psi_2 + \eta\psi_2 \\ \xi = \xi_M + \xi_K \\ \psi = \psi_{M1} + \psi_{M2} + \psi_2 \end{cases}$$

in Eq. (3.12): ξ_M, K – the stress and modulus of elasticity, ψ_{M1}, ψ_2 – instantaneous PW and CP of the sampled sandstone, ψ_{M2} – the PW of the randomly sampled sandstone, respectively.

The sandstone creep parameter confirmed by this method is non-linear, essentially refining the large module into a small portion of out-of-box morphology. The study and the obtained data will be subjected to residual squaring calculation as shown in Eq. (3.13) [24].

$$(3.13) \quad \Gamma = \sum_{i=1}^p (Y_i - f(X_i, d))^2$$

in Eq. (3.13): p – the number of observations, and d – a common variable for the squared residuals.

The first-order approximate equation can be written as Eq. (3.14) if the method is applied to find the minimal value of the residual square [25]. This equation is a fit to the sandstone UC, which can be safety performance of tunnels with abundant groundwater can be analyzed.

$$(3.14) \quad g(d^k + m^k) = g'(x, d^k) + A^k m^k$$

in Eq. (3.14): k – the number of iterations when the squared residuals take a minimal value. At the next iteration point, A^k – there exists a least squares solution to.

Under the condition that the value of A^k is known, there is Eq. (3.15) [26].

$$(3.15) \quad (U^k)_{LM} = (A^{k'} A^k + \Omega^k I)^{-1} A^{k'} e^k$$

in Eq. (3.15): $\Omega^k, \Omega^k I$ – the damping factor and the number of damping terms of the sandstone, $A^{k'}$ – the parameter in this process.

When $\Omega^k = 0$, the process solves for the optimal step size. As this value increases, the gradient of the model decreases. Studying the UC characteristics of sandstone samples under high CP and PW pressure is significant for tunnel construction. This study used numerical simulation to conduct in-depth experiments and aims to provide reliable methods for engineering design.

4. Examination of the effectiveness of ibm modeling of sandstone in a high-CP, high-PW environment

In order to verify the safety of the IBM model in tunnel sandstone UC under high CP and water pressure conditions, this study designs and conducts simulation experiments based on the IBM model and analyses its parameters. Finally, simulation experiments are conducted in Malm dataset.

4.1. Performance analysis of ibm's sandstone UC model under high CP and high PW conditions

This study divided the dataset into training set and test set with 20% and 80% respectively. The equipment used by the study are specifically shown in Table 1 [27].

When working in sandstone tunnels, the surrounding environment may have high CP and PW levels. The study processed the dataset for iterative optimization and plotted the iterative error versus ROC curve, as shown in Fig. 6.

Figure 6 shows the comparison graph of four models including IBM, YOLOv5, Golden Sine Algorithm (GS) and Long and Short-Term Memory network (LSTM) [28]. In Fig. 6, the lowest error rate value is found in the IBM model. In order to observe the loss rate and F1 value of the models, the study conducted experiments on both as in Fig. 7.

Table 1. Experimental parameters

Device type	Operating parameters or software
Quality of sandstone	312.5 g, 2115 g
Outside diameter of sandstone	30.57 mm, 220.14 mm
Longitudinal wave velocity of sandstone	1500.87 m/s, 10328.2 m/s
Main components of sandstone	Mica, quartz
Structure of sandstone	Fine scaly
Language	Easy Chinese
Deformation rate of machine	10^{-4} –100
Wave shape of machine	Normal, oblique, and trigonometric function wave
Static water flow of pump	6.2 mL/d
Computer chip	Intel i9 CPU
Model	Matlab R2020b
Data set	Malm

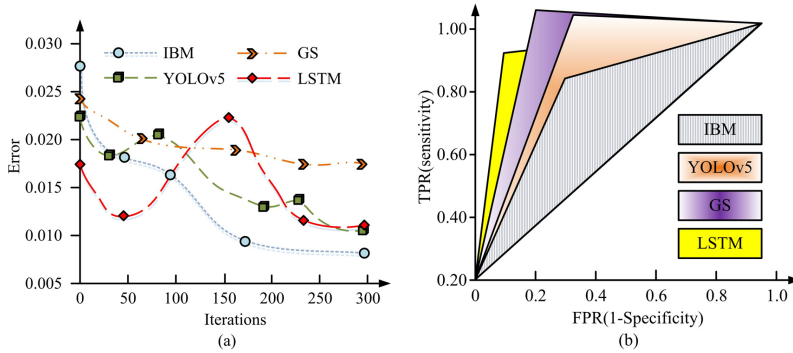


Fig. 6. Iterative error curve and ROC curve of the model; (a) Iterative error curves of four algorithms, (b) ROC curves of four algorithms

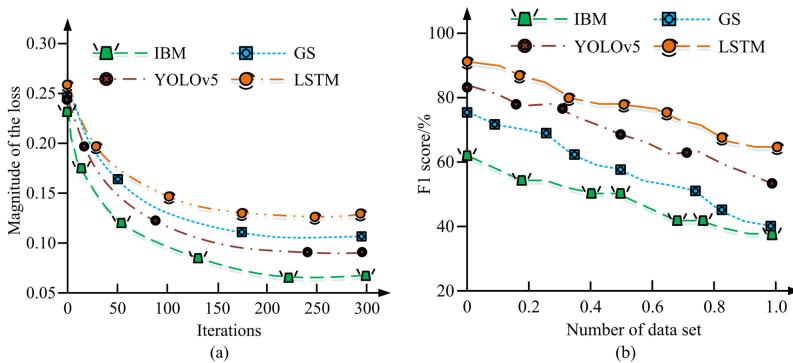


Fig. 7. Loss rate of four models and F1 value images; (a) Curve representing loss, (b) The value of F1

In Fig. 7 in the comparison between the loss rate and the F1 value, in the loss rate value the model shows 0.06, while the F1 value is as low as 40%, indicating that all the IBM models proposed in the study perform optimally.

4.2. Experimental verification of the effectiveness of IBM in safe construction in tunnel construction

In this study, after setting up the required parameters, simulation experiments were conducted on the Malm dataset. Two groups of sandstones of different sizes. These two pieces of sandstone were only subjected to the natural environment, as shown in Fig. 8 [29].

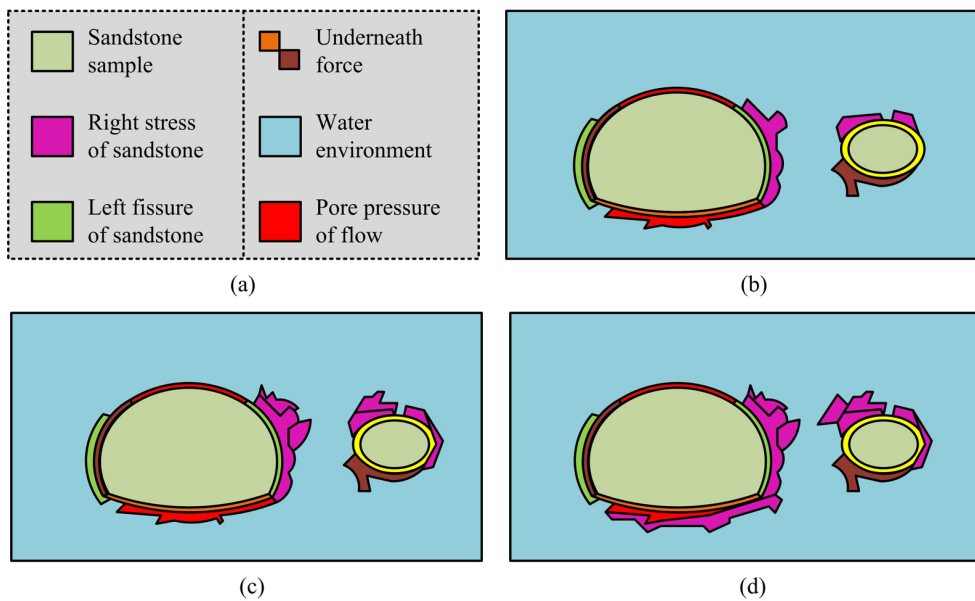


Fig. 8. Experimental results of sandstone control group; (a) Experimental legend, (b) Initial sandstone sample, (c) Sandstone ten days later, (d) Sandstone fifty days later

Fig. 8(a) is a legend of the experimental illustration, and Fig. 8(b), (c), and (d) show the changes of the sandstone as is and after ten and sixty days, respectively. In Fig. 8, both sandstones grow cracks of sandstone under the action of high CP and high PW. This study is based on four models to improve RS and draw the image of the improvement effect as Fig. 9.

In Fig. 9, the sandstone RS of all four experimental groups showed an increasing trend. This study was carried out to analyze the elastic modulus of sandstone under different seam water pressure and CP conditions, and plotted the images shown in Fig. 10.

Figure 10 shows the elastic modulus test results of sandstone under varying confining and PW pressures. The colors range from light to dark to indicate small to large elastic modulus values. Based on the experimental data in Fig. 10, an elastic modulus of over 20 GPa is necessary to impact the experimental outcomes. The study framework is presented in Fig. 11.

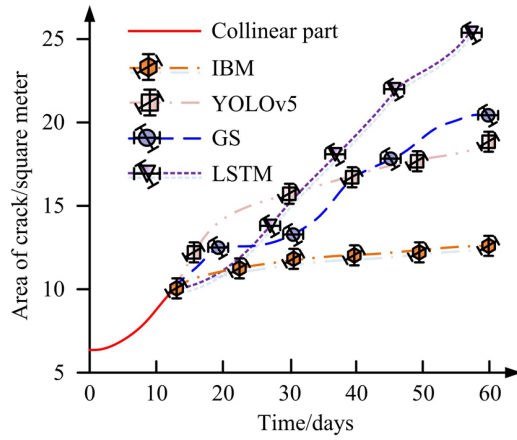


Fig. 9. Improvement effect diagram of sandstone fracture area of four models

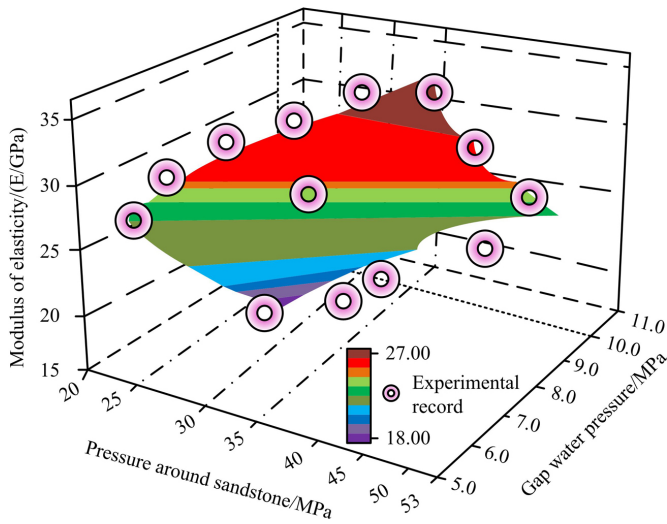


Fig. 10. Analysis of elastic modulus of sandstone

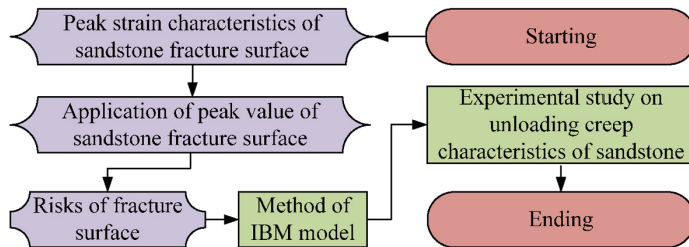


Fig. 11. Accurate and clear frame diagram

Figure 11 shows that the study of sandstone fracture surface can be divided into three parts. Firstly, the peak strain characteristics of the sandstone fracture surface are analyzed to understand the application of the peak value of the fracture surface. Next, the IBM model is established and simulated, and compared with the conventional model. Finally, the model's practicability is evaluated, and the next research direction is identified. The research makes two main contributions. Firstly, it studies elastic deformation to reduce deformation and stress concentration in tunnel structures, improving their stability when sandstone returns to its original state. Secondly, it examines creep deformation to reduce deformation and stress concentration in tunnel structures by slowly releasing the load under constant load, further improving their stability.

5. Conclusions

The research on the performance of sandstone UC is growing in popularity since tunneling technology advances quickly, which is important for ensuring construction workers' safety. In order to create an IBM model, its adaptability is underlined in the triaxial loading model, and it is rebuilt by Poisson's ratio. The IBM model can account for the nonlinear behavior of sandstone during unloading. The Malm dataset comprises experimental data collected by researchers. During the UC of sandstone, YOLO v5 can detect and track the target, enabling real-time monitoring and analysis of sandstone deformation. The IBM model performs favorably compared to YOLOv5, GS, and LSTM. According to the study's findings, the ideal performance was achieved with 182 iterations and a loss rate of 0.06. The ultimate crack area was reached by the sandstone in the control trial without external treatment after 10 days, at which point it already constitutes a safety risk to construction workers. The four models' retardation effects on sandstone UC in the control group studies where they were introduced were 200, 75, 60, and 41 days, respectively. This suggested that the IBM model can slow the rate of sandstone deterioration. The study found that it can have an impact on the experimental results after examining the modulus of elasticity of sandstone under various water pressure and CP settings. This study performed 36 experiments for sandstone UC and then produced a linear fit by comparing the results to the projected values in order to minimize this error. The experimental results indicate that the IBM model proposed in this study can effectively reduce the UC of sandstone under high CP and high PW conditions, which has a significant impact on worker safety during tunnel construction. However, the equipment is not suitable for high-temperature conditions. Therefore, this study primarily focuses on sandstone regions with abundant subterranean water sources nearby. With a linear fit value of 0.9827, the IBM was the control experiment among these 36 that came closest to the expected curve. Fit values for the other three models were 0.9548, 0.9756, and 0.9201. The experimental results indicate that the IBM model proposed in this study can effectively reduce the UC of sandstone under high CP and high PW conditions, which has a significant impact on worker safety during tunnel construction. However, the equipment is not suitable for high-temperature conditions. Therefore, this study primarily focuses on sandstone regions with abundant subterranean water sources nearby. Additionally, during building, geothermal impacts are frequently present. The future of research will go in this direction as equipment technology advances.

References

- [1] M. Varenik, J.C. Nino, E. Wachtel, S. Kim, and I. Lubomirsky, “Trivalent dopant size influences electrostrictive strain in ceria solid solutions”, *ACS Applied Materials and Interfaces*, vol. 13, no. 17, pp. 20269–20276, 2021, doi: [10.1021/acsami.0c20810](https://doi.org/10.1021/acsami.0c20810).
- [2] S.A. Rahman, E.D. Mitiku, S.B. Mule, G.T. Aduye, M.A. Huluka, and S. Mesfin, “Voltage sag mitigation using direct converter based DVR without error signal”, *Przegląd Elektrotechniczny*, vol. 97, no. 12, pp. 34–37, 2021, doi: [10.15199/48.2021.12.05](https://doi.org/10.15199/48.2021.12.05).
- [3] R. Perner, R. Schorn, and G. Atzl, “New construction of Albula Tunnel II—Experience with steel fibre shotcrete”, *Geomechanics and Tunneling*, vol. 14, no. 4, pp. 377–389, 2021, doi: [10.1002/geot.202100017](https://doi.org/10.1002/geot.202100017).
- [4] Y. Guo, Z. Mustafaoglu, and D. Koundal, “Spam detection using bidirectional transformers and machine learning classifier algorithms”, *Journal of Computational and Cognitive Engineering*, vol. 2, no. 1, pp. 5–9, 2023, doi: [10.47852/bonviewJCCE2202192](https://doi.org/10.47852/bonviewJCCE2202192).
- [5] Z. Dong, X. Zhang, C. Tong, X. Chen, H. Feng, and S. Zhang, “Grouting-induced ground heave and building damage in tunnel construction: A case study of Shenzhen metro”, *Underground Space*, vol. 7, no. 6, pp. 1175–1191, 2022, doi: [10.1016/j.undsp.2022.04.002](https://doi.org/10.1016/j.undsp.2022.04.002).
- [6] H. Jiang, J. Mu, J. Zhang, Y. Jiang, C. Liu, and X. Zhang, “Dynamic evolution in mechanical characteristics of complex supporting structures during large section tunnel construction”, *Deep Underground Science and Engineering*, vol. 1, no. 2, pp. 183–201, 2022, doi: [10.1002/dug2.12027](https://doi.org/10.1002/dug2.12027).
- [7] W. Zhu, G. Dai, W. Gong, and X.L. Zhao, “Study on unloading creep characteristics of the soil and application of the stress-dependent creep model in suction caisson foundation”, *China Ocean Engineering*, vol. 36, no. 1, pp. 123–132, 2022, doi: [10.1007/s13344-022-0011-1](https://doi.org/10.1007/s13344-022-0011-1).
- [8] Y. Wang, Y. Zhao, X. Ge, Y. Li, T. Huang, and Q. Zhang, “Calculation of drainage volume during tunnel construction based on the control of negative effects of ecosystem”, *Water Supply*, vol. 21, no. 3, pp. 1119–1226, 2021, doi: [10.2166/ws.2021.012](https://doi.org/10.2166/ws.2021.012).
- [9] Z. Zhang, “Study on ground deformation during Shield tunnel construction”, *Journal of Construction Research*, vol. 3, no. 2, 2021, doi: [10.30564/jcr.v3i2.4075](https://doi.org/10.30564/jcr.v3i2.4075).
- [10] D. Qiu, C. Qu, Y. Xue, B. Zhou, and J. Cui, “A comprehensive assessment method for safety risk of gas tunnel construction based on fuzzy bayesian network”, *Polish Journal of Environmental Studies*, vol. 29, no. 6, pp. 4269–4289, 2020, doi: [10.15244/pjoes/115979](https://doi.org/10.15244/pjoes/115979).
- [11] Y. Wang, H. Luo, and X.Y. Xiao, “Joint optimal planning of distributed generations and sensitive users considering voltage sag”, *IEEE Transactions on Power Delivery*, vol. 37, no. 1, pp. 93–104, 2022, doi: [10.1109/TPWRD.2021.3053996](https://doi.org/10.1109/TPWRD.2021.3053996).
- [12] T. Pan, “Influences of double-track shield tunnel construction on settlements of adjacent ground and buildings in a soft soil area”, *Hydrogeology and Engineering Geology*, vol. 49, no. 1, pp. 101–108, 2022, doi: [10.16030/j.cnki.issn.1000-3665.202106014](https://doi.org/10.16030/j.cnki.issn.1000-3665.202106014).
- [13] S. Oslund, C. Washington, A. So, and T. Chen, “Multiview robust adversarial stickers for arbitrary objects in the physical world”, *Journal of Computational and Cognitive Engineering*, vol. 1, no. 4, pp. 152–158, 2022, doi: [10.47852/bonviewJCCE2202322](https://doi.org/10.47852/bonviewJCCE2202322).
- [14] H.Y. He, W.H. Zhang, Y. Wang, and X.Y. Xiao, “A sensitive industrial process model for financial losses assessment due to voltage sag and short interruptions”, *IEEE Transactions on Power Delivery*, vol. 36, no. 3, pp. 1293–1301, 2021, doi: [10.1109/TPWRD.2020.3006017](https://doi.org/10.1109/TPWRD.2020.3006017).
- [15] X. Zheng, H. Zhang, and X. Su, “Construction technology of large-deformation High Geostress Soft rock tunnel”, *Journal of World Architecture*, vol. 5, no. 1, pp. 30–32, 2021, doi: [10.26689/jwa.v5i1.1875](https://doi.org/10.26689/jwa.v5i1.1875).
- [16] P. Clark, “Improvements to the observational method in New South Wales road tunnel construction”, in *Geotechnical Lessons Learnt—Building and Transport Infrastructure Projects. AGSSAS 2021*. Springer Nature Singapore, 2021, pp. 121–138, doi: [10.1007/978-981-99-1121-9_7](https://doi.org/10.1007/978-981-99-1121-9_7).
- [17] W.L. Hsu, Z. Ouyang, Z. Dong, F. Wu, C.Y. Chiu, and R. Liarnng, “Evaluation of procurement of environment monitoring equipment for tunnel construction”, *Sensors and Materials*, vol. 34, no. 6, pp. 2213–2227, 2022, doi: [10.18494/SAM3825](https://doi.org/10.18494/SAM3825).

- [18] S.M. Meye and Z. Shen, "Numerical simulation of the influence of tunnel construction by mining method on the seepage field in weathered granite stratum", *Engineering*, vol. 12, no. 6, pp. 424-456, 2020, doi: [10.4236/eng.2020.126031](https://doi.org/10.4236/eng.2020.126031).
- [19] L. Ü. Yuxiang, J. Yongjun, and W. Zheng, "Review on the hydrology and the ecological and environmental effects of tunnel construction in the karst valley of Southwest China", *Acta Ecologica Sinica*, vol. 40, no. 6, pp. 1851-1864, 2020, doi: [10.5846/stxb201810262312](https://doi.org/10.5846/stxb201810262312).
- [20] M. Ünver, M. Olgun, and E. Türkarslan, "Cosine and cotangent similarity measures based on Choquet integral for Spherical fuzzy sets and applications to pattern recognition", *Journal of Computational and Cognitive Engineering*, vol. 1, no. 1, pp. 21-31, 2022, doi: [10.47852/bonviewJCCE2022010105](https://doi.org/10.47852/bonviewJCCE2022010105).
- [21] C. Chen, T. Xu, G. Zhou, and T. Qin, "Experimental investigation of influence of alternating cyclic loadings on creep behaviors of sandstone", *Mechanics of Time-Dependent Materials*, vol. 25, no. 1, pp. 1-19, 2021, doi: [10.1007/s11043-019-09432-1](https://doi.org/10.1007/s11043-019-09432-1).
- [22] X. Pan, F. Berto, and X. Zhou, "Investigation of creep damage mechanical behaviors of red sandstone considering temperature effect", *Fatigue & Fracture of Engineering Materials and Structures*, vol. 45, no. 2, pp. 411-424, 2022, doi: [10.22541/au.162108952.29835546/v1](https://doi.org/10.22541/au.162108952.29835546/v1).
- [23] C. Sun, G. Li, M.E. Gomah, J. Xu, and H. Ron, "Experimental investigation on the nanoindentation viscoelastic constitutive model of quartz and kaolinite in mudstone", *International Journal of Coal Science and Technology*, vol. 8, no. 5, pp. 925-937, 2021, doi: [10.21203/rs.3.rs-30767/v1](https://doi.org/10.21203/rs.3.rs-30767/v1).
- [24] S. R. Taheri, A. Pak, S. Shad, et al., "Investigation of rock salt layer creep and its effects on casing collapse", *International Journal of Mining Science and Technology*, vol. 30, no. 3, pp. 357-365, 2020, doi: [10.1016/j.ijmst.2020.02.001](https://doi.org/10.1016/j.ijmst.2020.02.001).
- [25] X. Pan, F. Berto, and X. Zhou, "Creep mechanical characteristics and nonlinear viscoelastic-plastic creep model of sandstone after high temperature heat treatment", *Fatigue and Fracture of Engineering Materials and Structures*, vol. 46, no. 8, pp. 2982-3000, 2023, doi: [10.1111/ffe.14061](https://doi.org/10.1111/ffe.14061).
- [26] X.P. Zhou, F. Shen, and F. Berto, "Experimental study on triaxial creep behavior of red sandstone under different pore pressures based on ultrasonic measurement", *Fatigue & Fracture of Engineering Materials & Structures*, vol. 45, no. 8, pp. 2388-2402, 2022, doi: [10.1111/ffe.13753](https://doi.org/10.1111/ffe.13753).
- [27] J. Wang, J. Li, and Z. Shi, "Crack evolution law and failure mode of red sandstone under fatigue-creep interaction", *Fatigue & Fracture of Engineering Materials & Structures*, vol. 45, no. 1, pp. 270-284, 2022, doi: [10.1111/ffe.13599](https://doi.org/10.1111/ffe.13599).
- [28] C.P. Wen and X.Q. Yuan, "Hyperbolic consolidation creep model of weathered red sandstone coarse-grained soil under the wet and dry cycles conditions", *Geotechnical and Geological Engineering*, vol. 40, no. 10, pp. 5103-5113, doi: [10.1007/s10706-022-02202-w](https://doi.org/10.1007/s10706-022-02202-w).
- [29] W. Jing, Y.L. Gao, R.C. Jin, and L.W. Jing, "Deformation failure analysis and identification method of zoning type of actual tunnel surrounding rock", *Archives of Civil Engineering*, vol. 69, no. 4, pp. 549-571, doi: [10.24425/ace.2023.147676](https://doi.org/10.24425/ace.2023.147676).

Received: 2023-07-31, Revised: 2024-01-30